Electronic structures of $CuFeS_2$ and $CuAl_{0.9}Fe_{0.1}S_2$ studied by electron and optical spectroscopies

M. Fujisawa
Synchrotron Radiation Laboratory, Institute for Solid State Physics, The University of Tokyo, Tanashi, Tokyo 188, Japan

S. Suga
Department of Material Physics, Faculty of Engineering Science, Osaka University, Toyonaka, Osaka 560, Japan

T. Mizokawa and A. Fujimori
Department of Physics, The University of Tokyo, Bunkyo-ku, Tokyo 113, Japan

K. Sato
Faculty of Technology, Tokyo University of Agriculture and Technology, Koganei, Tokyo 184, Japan
(Received 4 October 1993)

The electronic structures of the chalcopyrite-type $CuFeS_2$ and $CuAl_{0.9}Fe_{0.1}S_2$ are studied by x-ray photoemission (XPS), resonance photoemission, Auger-electron, optical reflectance, and electron-energy-loss (EELS) spectroscopies. The Fe $3d$-derived states are revealed by the valence-band XPS spectra and the Fe $3p$ core resonance photoemission spectra. The spectra are analyzed by configuration-interaction calculation on the FeS_4 cluster model; the analysis yields the S $3p \rightarrow$ Fe $3d$ charge-transfer energy Δ close to zero, indicating strong covalency between the Fe $3d$ and S $3p$ orbitals. This situation is reflected upon the reduced Fe magnetic moment and the high Neel temperature of $CuFeS_2$. The S $3p \rightarrow$ Fe $3d$ charge-transfer excitation is resolved in the optical reflectance and EELS spectra, which explains the larger binding-energy tails of the core-level photoemission spectra of $CuFeS_2$. The Cu $3d$ two-hole bound state is studied through the Cu $L_3M_{4,5}M_{4,5}$ Auger and Cu $3p$ core resonance photoemission spectra, from which the effective Coulomb energy $U_{\rm eff}(^1G)$ between the two holes and the Cu $3d \rightarrow 4sp$ promotion energy $\Delta_{d\text{-}sp}$ are evaluated. The Cu $2p$ core XPS spectrum of $CuFeS_2$ has revealed a mixing of the d^9 ("Cu^{2+}") configuration into the formally monovalent Cu. This is interpreted as due to the Cu $3d$–Fe $3d$ hybridization mediated by the S $3sp$ valence states.

I. INTRODUCTION

Chalcopyrite-type I-III-VI_2 compounds (I=Cu,Ag; III=Al,Ga,In; VI=S,Se,Te) are materials quite useful for practical applications such as solar batteries, nonlinear optical devices, and luminescence diodes.[1] Their electronic structures are also of interest in that they are ternary semiconductors based on the diamond structure: The chalcopyrite structure is obtained by replacing the group-II atoms in the II-VI zinc-blende lattice by atoms of group I (Cu,Ag) and III (Al,Ga,In). The valence-band structures of some Cu-based chalcopyrites were previously investigated by x-ray photoemission spectroscopy (XPS).[2] The larger binding energy (E_B) side of the prominent Cu $3d$ band centered at $E_B=2.5-3$ eV was attributed to the ns and np states of the group-III atoms; the states closer to the Fermi level were assigned to hybridized states between the Cu $3d$ and the p state of the group-VI atoms. These assignments were supported by band-structure calculations made by the discrete variational-$X\alpha$ (DV-$X\alpha$) method on $CuAlS_2$ and $CuGaS_2$.[3]

Among the Cu-based chalcopyrite-type compounds, $CuFeS_2$ has unique optical, electrical, and magnetic properties,[4–6] Evaporated thin films of $CuFeS_2$ and $CuAlS_2$ (unintentionally doped with Fe) have shown strong absorption starting from 0.6 and 3.3 eV, respectively. Because photoconductivity was observed above these energies, the empty states involved in the optical absorption are assigned to the conduction band.[4] The temperature dependence of the electric conductivity and the temperature independence of the carrier concentration in $CuFeS_2$ suggested metallic behavior although the conductivity was small [$10^3\ \Omega^{-1}\,cm^{-1}$ at 100 K (Ref. 5)] compared with that of typical metals. It was also found that the thermoelectric power was unusually large (480 μV/K),[5] From these results, $CuFeS_2$ was rather considered as a degenerate semiconductor.[5] There is also a recent proposal that $CuFeS_2$ is a zero-gap semiconductor.[7] $CuFeS_2$ is an antiferromagnet with an extremely high Neel temperature $T_N=823$ K; the ordered magnetic moment of the Fe atom is $3.85\pm0.2\mu_B$,[6] which is much smaller than that of the free Fe^{3+} (d^5) ion $5\mu_B$. The above results indicate that the Fe $3d$ states in $CuFeS_2$ are considerably delocalized or strongly hybridized with the S $3sp$ states.[5]

The electronic band structure of $CuFeS_2$ was first studied by an optical reflectance measurement and its Kramers-Kronig analysis in the photon energy range from 0.0025 to 6 eV.[8] In the absorption spectrum, two narrow bands were observed at $\sim$1 and $\sim$2 eV and another broad band was observed at $\sim$6 eV. The first two narrow bands were assigned to the optical transition from the top of the valence band to two conduction bands. The band structures were calculated by the DV-

$X\alpha$ method for some Cu-based chalcopyrites including $CuFeS_2$.[3,9] In contrast to the case of $CuXS_2$ (X=Al,Ga),[3] the Fe $3d$ states in $CuFeS_2$ are predicted to be strongly hybridized with other valence states and spread over the whole valence-band region.[9] Photoemission spectra were measured by use of synchrotron radiation.[10] The energy distribution curves of the valence-band spectra and the Fe $3p \rightarrow 3d$ resonance photoemission spectra have qualitatively supported the general features of the band-structure calculations.

Although photoemission spectroscopy is a powerful means to investigate the valence-band structures, one should notice that the photoemission spectra actually provide electron-removal spectra and that they do not necessarily represent the one-electron band structure of the ground state, especially for systems with strong electron-electron interaction or strong electron correlation such as transition-metal compounds. Because of this fact, proper analysis of the photoemission spectra can give considerable insight into the electron correlation as well as on the orbital hybridization in the transition-metal compounds. In this paper, we have studied not only the valence band but also core levels of $CuFeS_2$ and $CuAl_{0.9}Fe_{0.1}S_2$ by means of various types of electron and optical spectroscopies. The experimental results are compared with those of other Cu compounds as well as with configuration-interaction (CI) calculation on the $(FeS_4)^{5-}$ cluster model, in which not only the initial ground state but also the electron-removal final states are explicitly considered.

II. EXPERIMENT

Measurements of optical reflectance and ultraviolet photoemission spectroscopy (UPS) were performed using synchrotron radiation from SOR-RING, a 0.4-GeV electron storage ring of the Institute for Solid State Physics of the University of Tokyo. For the reflectance measurement, monochromatic light through a 1-m Seya-Namioka monochromator was used in a geometry with the incidence angle of 22.5°. The reflected light was detected by a photomultiplier coated with sodium salicylate. The present measurement was performed in the photon energy range from 4 to 25 eV with a wavelength resolution of 0.3 nm. The spectrum in the photon energy range below 6 eV was taken from Oguchi, Sato, and Teranishi.[8] These spectra were combined and analyzed by the Kramers-Kronig transformation to obtain the dielectric constants ϵ_1, ϵ_2, and the loss function $\mathrm{Im}(-1/\epsilon)$.

For the UPS measurement performed with use of synchrotron radiation, a spectrometer with a double-pass cylindrical-mirror analyzer (DCMA) connected to a modified Rowland-mount monochromator was used. The overall resolution was set to ~0.5 eV at the photon energy of $\hbar\omega$=70 eV. XPS measurement was carried out in a separate system with a Mg $K\alpha$ x-ray source ($\hbar\omega$=1253.6 eV). The electron-energy-loss spectra (EELS) were measured in the same apparatus with use of a grazing-incidence electron gun (with the primary electron energy of 2 keV). The energies of electrons were analyzed using a DCMA with the overall energy resolution of ~1 eV for XPS and ~0.7 eV for EELS.

For the optical reflectance measurement of $CuFeS_2$, an as-grown surface of a single crystal obtained by the chemical vapor transport[5] was used. For the photoemission measurement, the samples obtained by the Bridgman method were used. $CuAl_{0.9}Fe_{0.1}S_2$ was studied instead of $CuAlS_2$ because the presence of the Fe ions reduced the charging effect which hinders a reliable measurement of photoemission spectra. Clean surfaces for the photoemission measurements were obtained by scraping the samples with a diamond file in the vacuum of $\sim 1\times10^{-10}$ Torr.

III. RESULTS

Figure 1 shows the photoemission spectra of $CuFeS_2$ in the valence-band region for photon energies in the Fe $3p$ core excitation region. Binding energies E_B's are referred to the top of the valence band. The spectra consist of a shoulder at E_B=1 eV, a prominent peak at E_B=3 eV, an inconspicuous shoulder around 5 eV, and a weak hump at E_B=14 eV. In Fig. 1, the corresponding features in the spectra are connected by vertical lines. In addition, a very weak hump which can be identified around $E_B \sim 11$ eV from a difference spectrum of the XPS spectra between $CuFeS_2$ and $CuAl_{0.9}Fe_{0.1}S_2$ is also marked (see below). The line shape of the whole spectra appreciably changes with $\hbar\omega$ from $\hbar\omega$=53 to 58 eV. The constant-initial-state (CIS) spectra at various E_B's are shown in Fig. 2 together with the partial yield spectrum (measured

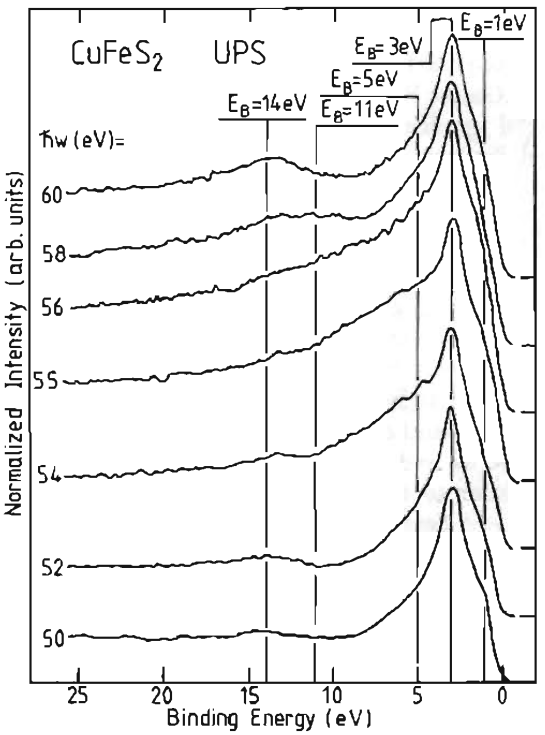

FIG. 1. Photoemission spectra of $CuFeS_2$ in the Fe $3p$ core excitation region. Photon energies are given on the left-hand side. The E_B's show the binding energies of the structures discussed in the text.

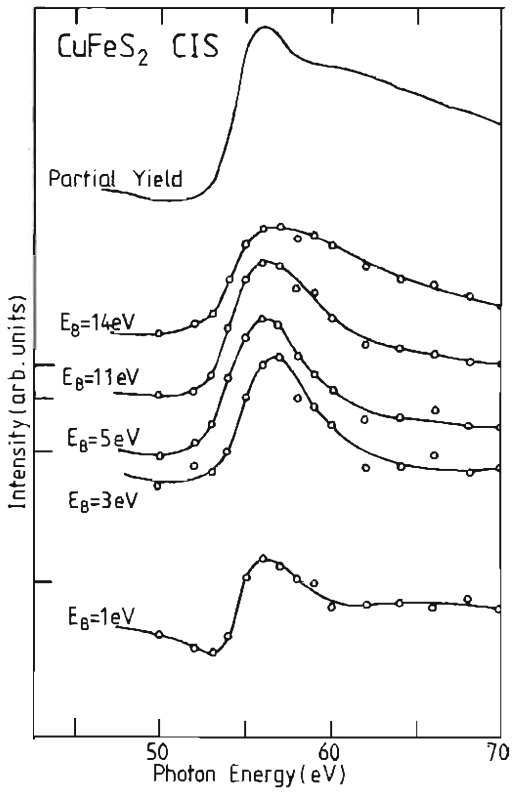

FIG. 2. CIS spectra of $CuFeS_2$ evaluated from the result in Fig. 1.

at the kinetic energy of $E_K = 5$ eV), which is thought to represent the absorption spectrum. The CIS spectrum for $E_B = 1$ eV has a typical Fano-type line shape with a dip below the Fe $3p$ core threshold followed by the peak at $\hbar\omega \sim 56$ eV, while the other CIS spectra do not show the dip structure. The resonance effect was not clearly resolved in $CuAl_{0.9}Fe_{0.1}S_2$ at the Fe $3p$ threshold because of the low Fe concentration.

The valence-band XPS spectra of $CuAl_{0.9}Fe_{0.1}S_2$ and $CuFeS_2$ are shown in Figs. 3(a) and 3(b), respectively. Binding energies have been calibrated using the Au $4f_{7/2}$ core peak. The dots in Fig. 3(c) show the difference spectrum between these two spectra after having normalized the spectral intensities to the integrated intensity of the S $2p$ core XPS peak and having shifted the $CuAl_{0.9}Fe_{0.1}S_2$ spectrum so as to align the Cu $3d$ peaks of the two spectra. The difference spectrum thus obtained largely represents the contribution from the Fe $3d$ states since the photoemission cross section of the Fe $3d$ state is much larger than those of the Al $3p$ states at this photon energy. (Fe $3d$, Al $3p$, and Al $3s$, cross sections are estimated as 5×10^{-3}, 1×10^{-3}, and less than 1×10^{-4} Mb,[11] respectively.) Prominent contribution from the Fe $3d$ states is revealed around $E_B = 1$ and 5 eV with weaker contribution around $E_B = 11$ eV. The binding energies of these structures are marked in Fig. 1 and the corresponding CIS spectra are given in Fig. 2. The difference spectrum between the two UPS spectra taken at the resonance maximum ($\hbar\omega = 56$ eV) and the resonance minimum ($\hbar\omega = 53$ eV) (Fig. 1) also shows similar structures at $E_B \sim 1$–5 and 11 eV. However, the intensity around $E_B = 11$ eV is higher than that in the difference XPS spectrum probably because of the complicated intensity modulation of the Fano type in the resonance photoemission spectra. In the following analysis, we will therefore use the difference XPS spectrum as a measure of the Fe $3d$-derived states.

The Fe $2p$ core XPS spectrum of $CuFeS_2$ is shown in Fig. 4. The $2p_{3/2}$ component at $E_B = 708$ eV shows remarkable asymmetry with a tail toward larger E_B. The satellite observed on the larger E_B side of the $2p_{1/2}$ component at $E_B \sim 730$ eV is assigned to a plasmon satellite accompanying the $2p_{3/2}$ peak because the splitting from the main peak is close to the bulk plasmon energy obtained from the EELS spectrum.

In Fig. 5, the Cu $2p$ core spectra of $CuFeS_2$ and $CuAl_{0.9}Fe_{0.1}S_2$ are compared with those of other Cu compounds with known formal valences.[12–14] The energy positions of the $2p_{3/2}$ and $2p_{1/2}$ peaks are $E_B = 932.3$ and 952.0 eV for both $CuFeS_2$ and $CuAl_{0.9}Fe_{0.1}S_2$ whereas the spectral line shape is slightly different from each other. Namely, $CuFeS_2$ shows a weak tail for both the Cu $2p_{3/2}$

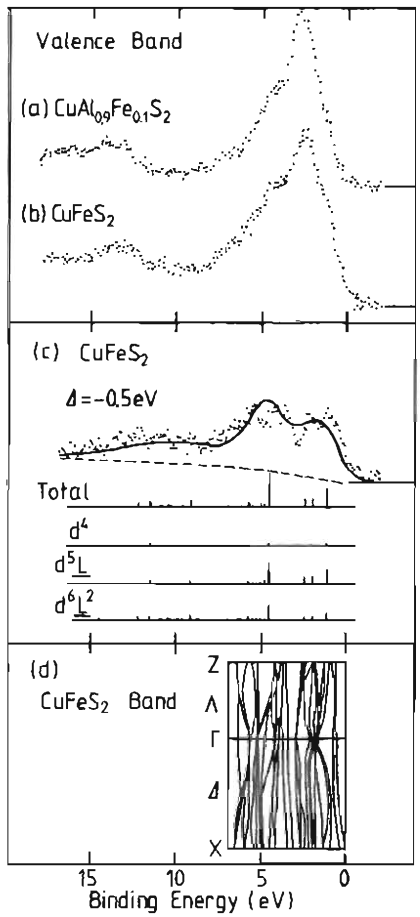

FIG. 3. XPS spectra of (a) $CuAl_{0.9}Fe_{0.1}S_2$ and (b) $CuFeS_2$ in the valence-band region. (c) Dots: (b)−(a) difference spectrum. Bar diagrams: results of the cluster-model CI calculation. Solid curve: Fe $3d$-derived contribution obtained by the cluster-model calculation appropriately broadened and superimposed to a smooth background (dashed line).

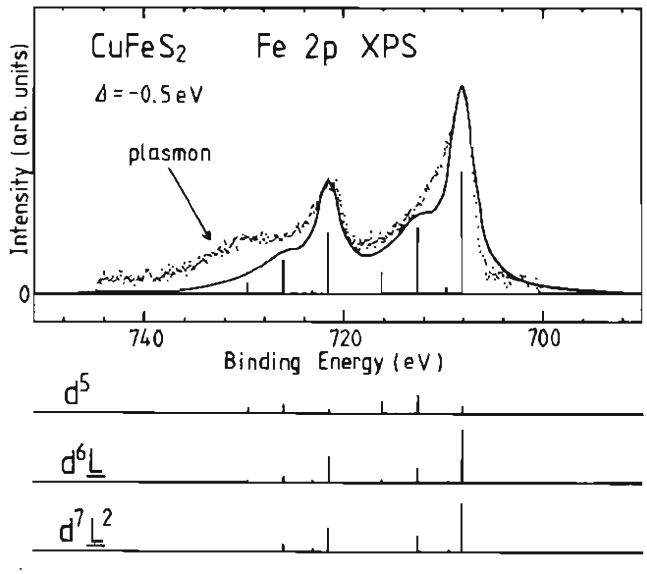

FIG. 4. Fe $2p$ core XPS spectrum (dots) and its cluster-model analysis (solid curve).

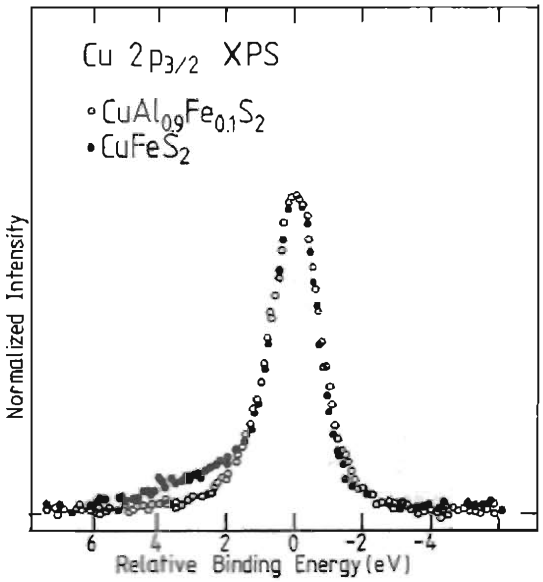

FIG. 6. Cu $2p_{3/2}$ core XPS spectra of $CuFeS_2$ and $CuAl_{0.9}Fe_{0.1}S_2$. The peak heights and the peak binding energies are aligned.

and $2p_{1/2}$ peaks toward larger E_B. This is more clearly seen in Fig. 6, where the $2p_{3/2}$ spectra of both compounds are shown on an expanded scale after subtracting a linear background. A similar tail is also recognized in the S $2p$ core XPS spectrum as shown in Fig. 7. Figure 5 shows that the spectra of the formally "di" and "trivalent" Cu compounds (CuO and $NaCuO_2$, respectively) have well-defined satellites on the larger binding energy side of the Cu $2p$ main peak. On the contrary, no clear satellite is observed in the spectra of the formally "monovalent" compound (Cu_2O). We thus conclude that the Cu ion in both $CuFeS_2$ and $CuAl_{0.9}Fe_{0.1}S_2$ is basically in the monovalent or "Cu^+" state. A modification of this simplest picture, however, will be given in Sec. IV.

In order to complement the information from the Cu $2p$ core photoemission, the Cu $L_3M_{4,5}M_{4,5}$ Auger spectra are measured as shown in Fig. 8. It is found that the peaks are located at different kinetic energies of $E_K = 918.2$ and 916.8 eV for $CuFeS_2$ and $CuAl_{0.9}Fe_{0.1}S_2$, respectively. Both the $CuFeS_2$ and $CuAl_{0.9}Fe_{0.1}S_2$ spectra show a sharp central peak and humps on its both sides.

Figures 9 and 10 show the resonance photoemission behavior in the valence bands of $CuFeS_2$ and $CuAl_{0.9}Fe_{0.1}S_2$ in the Cu $3p$ core excitation region. We find clear satellite structures at $E_B = 14.8$ and 15.9 eV for $CuFeS_2$ and $CuAl_{0.9}Fe_{0.1}S_2$, respectively. These values

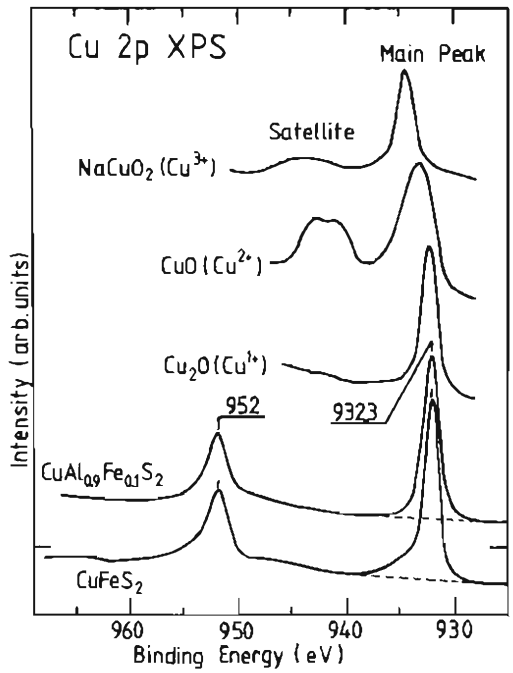

FIG. 5. Cu $2p$ core XPS spectra of $CuFeS_2$ and $CuAl_{0.9}Fe_{0.1}S_2$ compared with the Cu $2p_{3/2}$ XPS of other reference materials with formal valences "Cu^{3+}," "Cu^{2+}," and "Cu^+."

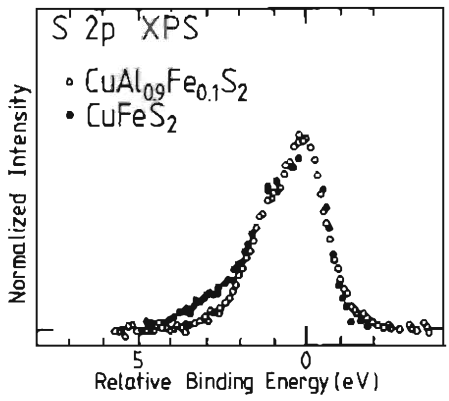

FIG. 7. S $2p$ core XPS spectra of $CuFeS_2$ and $CuAl_{0.9}Fe_{0.1}S_2$. The peak heights and the peak binding energies are aligned.

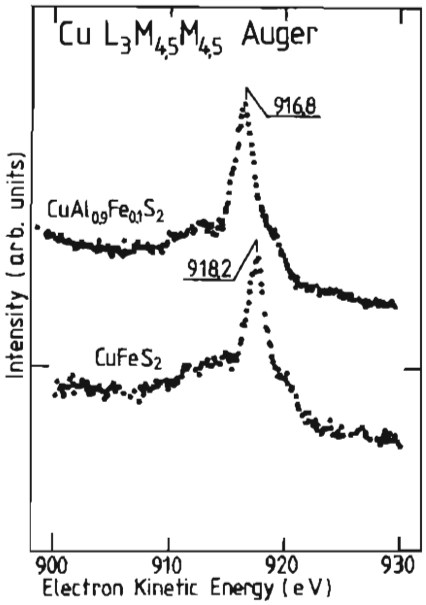

FIG. 8. Cu $L_3M_{4,5}M_{4,5}$ Auger spectra of $CuFeS_2$ and $CuAl_{0.9}Fe_{0.1}S_2$.

are similar to those observed in Cu metal and other monovalent Cu compounds.[13] The CIS spectra of the satellites and the valence-band peaks are shown in Fig. 11, where the intensities are tentatively normalized at $\hbar\omega = 70$ eV. A clear resonance enhancement is observed for the satellites whereas the resonance behavior of the

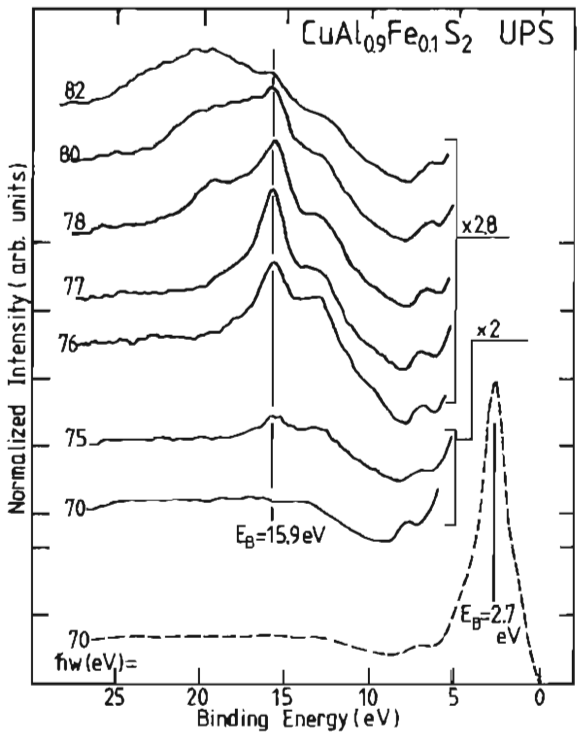

FIG. 10. Photoemission spectra of $CuAl_{0.9}Fe_{0.1}S_2$ in the Cu $3p$ core excitation region. Photon energies are given on the left-hand side. The E_B's of the valence-band peaks and the satellites are given.

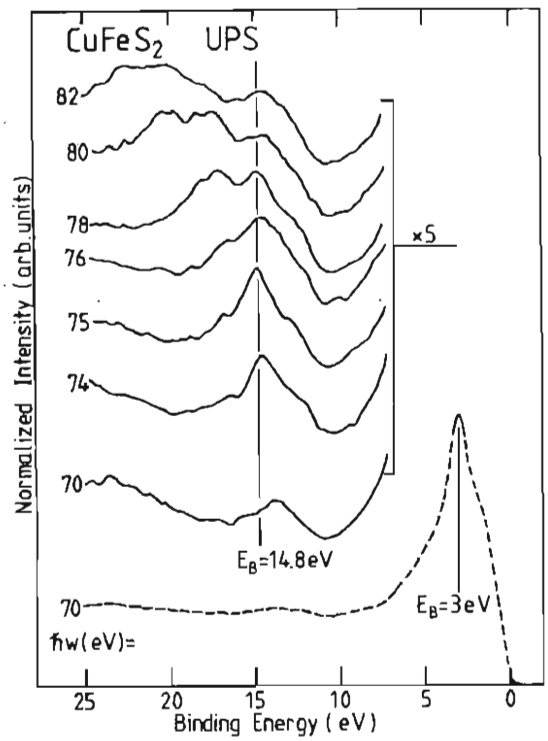

FIG. 9. Photoemission spectra of $CuFeS_2$ in the Cu $3p$ core excitation region. Photon energies are given on the left-hand side. The E_B's of the valence-band peaks and the satellites are given.

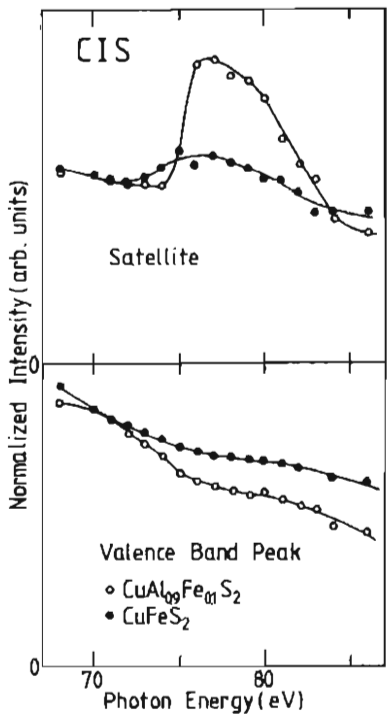

FIG. 11. CIS spectra of the Cu $3d$ satellites ($E_B = 14.8$ and 15.9 eV) and the valence-band peaks ($E_B = 3$ and 2.7 eV) for $CuFeS_2$ and $CuAl_{0.9}Fe_{0.1}S_2$, respectively.

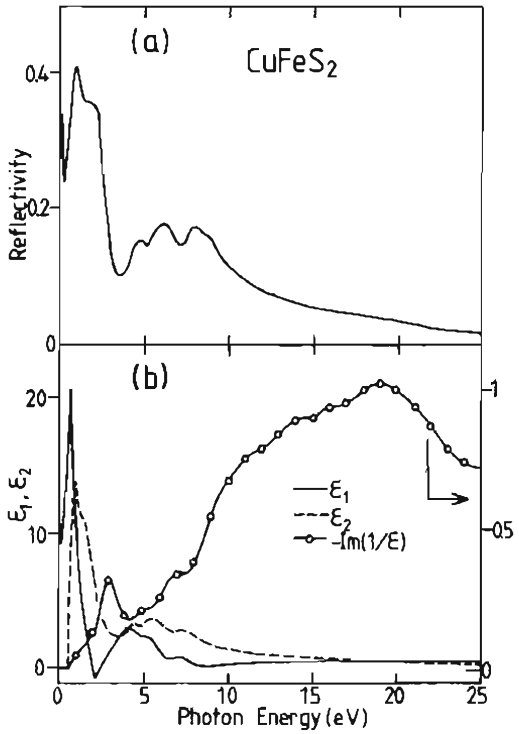

FIG. 12. (a) Reflectivity spectrum of $CuFeS_2$. (b) Dielectric constants ϵ_1, ϵ_2, and the loss function $\mathrm{Im}(-1/\epsilon)$ of $CuFeS_2$ obtained by the Kramers-Kronig transformation of the reflectivity spectrum.

valence-band peaks is much less obvious.

The optical reflectance spectrum of $CuFeS_2$ in the photon energy range from 0.2 to 25 eV is shown in Fig. 12(a). The dielectric constants ϵ_1, ϵ_2, and the loss function $-\mathrm{Im}(1/\epsilon)$ are obtained by the Kramers-Kronig analysis of the reflectance spectrum as shown in Fig. 12(b). A sharp peak at $\hbar\omega=3$ eV and a broad peak around $\hbar\omega=20$ eV are revealed in the loss function.

The directly measured EELS spectra of both materials are shown in Fig. 13, with the intensities normalized to the height of the primary electron peak. Both spectra have a large, broad peak around 20 eV. In addition, a sharp peak is observed at the loss energy of 3 eV for $CuFeS_2$, in agreement with the loss function derived from the optical reflectance spectrum. One also notices that the 3-eV peak is absent in $CuAl_{0.9}Fe_{0.1}S_2$.

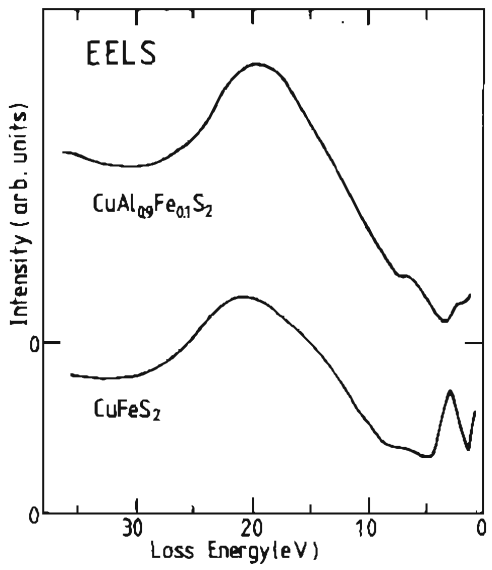

FIG. 13. EELS spectra of $CuFeS_2$ and $CuAl_{0.9}Fe_{0.1}S_2$ for the primary electron energy of 2 keV. The intensities are normalized to the height of the primary electron peak.

IV. DISCUSSION

A. CI cluster model

Before going into detailed discussions of the experimental results, a framework of the CI cluster-model analysis is briefly given.[15] The calculation treats several electronic configurations with different d-electron numbers both in the initial and final states of photoemission. The parameters characterizing the electronic structure are (i) the charge-transfer energy Δ, the energy required for the ligand $p\rightarrow$ metal d charge transfer, i.e., for $d^n\rightarrow d^{n+1}\underline{L}$, where $\underline{L}$ denotes a ligand hole; (ii) the d-d Coulomb energy U; and (iii) the p-d transfer integrals $(pd\sigma)$ and $(pd\pi)$. The present calculation was done on the $(FeS_4)^{5-}$ cluster. For $n=5$ corresponding to the formal valence of Fe^{3+} $(3d^5)$, the ground-state wave function has the form

$$\Psi_g=a|d^5\rangle+b|d^6\underline{L}\rangle+c|d^7\underline{L}^2\rangle\ . \tag{1}$$

The final state of the Fe $3d$ photoemission is given by

$$\Psi_f=a_1|d^4\rangle+b_1|d^5\underline{L}\rangle+c_1|d^6\underline{L}^2\rangle \tag{2}$$

and that of the Fe $2p$ core-level XPS by

$$\Psi_f=a_2|\underline{2p}d^5\rangle+b_2|\underline{2p}d^6\underline{L}\rangle+c_2|\underline{2p}d^7\underline{L}^2\rangle\ , \tag{3}$$

where $\underline{2p}$ stands for the $2p$ core hole. Optimum values for Δ, U, and $(pd\sigma)$ are determined by fitting the calculated Fe $3d$-derived spectrum and the Fe $2p$ core XPS spectra to the experimental ones. [The ratio $(pd\sigma)/(pd\pi)$ has been fixed at -2.2 throughout the calculation.[15–17]]

Here we note that Δ and U are defined with respect to the center of gravity of the multiple of each configuration whereas one can also define the charge-transfer energy and the d-d Coulomb energy with respect to the lowest states of the corresponding multiplets. They are referred to as Δ_{eff} and U_{eff} hereafter. Values for Δ_{eff} and U_{eff} rather than Δ and U are more directly reflected upon measured physical quantities such as band gaps and charge-transfer excitation energies.

B. Electron-energy-loss satellite

It is found for $CuFeS_2$ that both the EELS spectrum and the loss function $-\mathrm{Im}(1/\epsilon)$ obtained by the Kramers-Kronig analysis of the reflectance spectrum have a peak at 3 eV, corresponding to the ϵ_2 peaks at 1–2 eV. Since no corresponding feature is observed in the

EELS spectrum of $CuAl_{0.9}Fe_{0.1}S_2$, this structure should have its origin in the Fe $3d$ states. We interpret the structure as due to interband transitions (charge-transfer excitation) from the S $3p$- to Fe $3d$-dominated band states. We have pointed out above that the Cu $2p$ and S $2p$ core XPS spectra of $CuFeS_2$ have an appreciable tail toward larger E_B compared with those of $CuAl_{0.9}Fe_{0.1}S_2$ (Figs. 6 and 7). It is likely that these tails are energy-loss satellites due to the S $3p \rightarrow$ Fe $3d$ excitation. The large oscillator strength of the charge-transfer excitation indicates that the S $3p$–Fe $3d$ bonding is substantially covalent.

The broad EELS peak around 20 eV is due to the bulk plasmon excitation. Corresponding satellites are observed for the Fe $2p$ core XPS spectrum of $CuFeS_2$ (Fig. 4).

C. Valence-band and Fe 3d states in $CuFeS_2$

Typical valence-band structures of the present compounds are revealed by the XPS spectra and off-resonance UPS spectra as shown in Figs. 3(a) and 3(b) and at the bottom of Figs. 1, 9, and 10. The prominent peak recognized around $E_B = 3$ eV is due to the Cu $3d$ states, being judged from its common spectral line shape in both compounds as well as from the larger cross section of the Cu $3d$ states than those of the S $3sp$ and the Al $3sp$ states in XPS. The weak hump around $E_B = 14$ eV in the off-resonance spectra (Figs. 9 and 10) is assigned to the S $3s$ state. Both the Cu $3d$ and S $3sp$ components cancel in the difference XPS spectrum as demonstrated in Fig. 3(c). The Fe $3d$-derived states thus obtained in the difference spectrum show the structures around $E_B = 1$, 5, and 11 eV. The band structure of $CuFeS_2$ calculated with the DV-$X\alpha$ method by Hamajima *et al.*[9] is also shown in Fig. 3(d) for comparison. One can see that while the band structure well explains the structures around $E_B = 1$ and 5 eV, the third structure around $E_B = 11$ eV is not present in the calculated band structure.[18]

The Fe $3d$-derived spectrum obtained by the CI cluster-model calculation is shown in the lower part of Fig. 3(c). The calculated line spectra have been convoluted with a Lorentzian function with a full width at half maximum (FWHM) of $0.15E_B$ to simulate the lifetime broadening and with a Gaussian function (FWHM of 1 eV) to simulate the instrumental broadening. The resulting spectrum is superimposed to a smooth background (dashed line) due to secondary electrons and is shown by a solid curve in Fig. 3(c). From this analysis, we find that the charge-transfer energy $\Delta = -0.5 \pm 0.5$ eV, the d-d Coulomb energy $U = 4.0 \pm 1.0$ eV, and the transfer integral $(pd\sigma) = 1.5 \pm 0.2$ eV. The decomposition of the calculated spectrum into the d^4, $d^5\underline{L}$, and $d^6\underline{L}^2$ final-state components shown in Fig. 3(c) indicates that the main features around $E_B = 1$ and 5 eV are predominantly $d^5\underline{L}$ and $d^6\underline{L}^2$-like, whereas the feature around $E_B = 11$ eV has significant d^4 character. The Fe $2p$ core XPS spectrum has also been calculated using the same Δ and U values as shown in Fig. 4. The good agreement between theory and experiment for the Fe $2p$ XPS confirms the validity of the model and the parameter values.

The small Δ indicates strong hybridization between the Fe $3d$ and S $3p$ states in $CuFeS_2$ and Fe-doped chalcopyrite-type compounds, whereas the large U indicates that the Fe $3d$-$3d$ Coulomb correlation, which is not properly taken into account in the band-structure calculation, remains quite important even under the strong Fe $3d$–S $3p$ hybridization.

In the UPS spectra in the Fe $3p$ core excitation region, the whole valence band of $CuFeS_2$ shows resonant enhancement as shown in Figs. 1 and 2, revealing that Fe $3d$ states are spread over the whole valence-band region. Such an enhancement is usually explained as due to the interference between direct photoemission from the Fe $3d$ valence states and the discrete Fe $3p \rightarrow 3d$ core excitation followed by the direct recombination process. The CIS spectrum at $E_B = 1$ eV has a prominent dip below the $3p$ excitation threshold and therefore the $E_B = 1$ eV feature is ascribed to the $d^5\underline{L}$ (and $d^6\underline{L}^2$) final states, consistent with the cluster-model analysis. The CIS spectra at larger E_B's show a prominent peak above the threshold with no clear dip and reflect the sizable amount of d^4 contribution around $E_B = 11$ eV.

The present estimate of the charge-transfer energy $\Delta = -0.5 \pm 0.5$ eV is considerably smaller than those ($\Delta \sim 2$–3 eV) of the ternary magnetic semiconductors $Cd_{1-x}Mn_xY$ (Y=S, Se, and Te).[16] This small Δ is a result of the combined effects of the increased atomic number (Mn to Fe) and valence (2+ to 3+) of the $3d$ transition element.[17] On the other hand, Δ_{eff} is larger than Δ by ~ 2.6 eV and is therefore positive ($\Delta_{eff} = 2.1 \pm 0.5$ eV) because the lowest component of the d^5 multiplet is located far below the center of gravity of the multiplet due to the strong exchange stabilization of the half-filled d^5 configuration. This value is close to the energies of the charge-transfer excitation in $CuFeS_2$ which is ascribed to the peaks around 1–2 eV in the ϵ_2 spectrum (Fig. 12). The strong Fe-S covalency increases the net d-electron number on the Fe atom from the ionic value 5 to 5.55 ± 0.1 due to the transfer of electrons into the empty (minority-spin) $3d$ orbitals. Accordingly, the ordered magnetic moment of the Fe atom is reduced from $5\mu_B$ to $4.45 \pm 0.1\mu_B$. If we take into account the nonorthogonality between the Fe $3d$ and S $3p$ atomic orbitals, part of the electronic charges and spin density is distributed on the Fe-S bonds and consequently we obtain the net d-electron number of 4.6 ± 0.1 and the Fe magnetic moment $3.8 \pm 0.1\mu_B$, in excellent agreement with the experimental value of $3.85 \pm 0.2\mu_B$.[6] We also note that the small Δ_{eff} qualitatively explains the extremely high Neel temperature of $CuFeS_2$ because the antiferromagnetic coupling strength between neighboring Fe spins is proportional to $\sim \Delta_{eff}^{-2}(1/\Delta_{eff} + 1/U_{eff})$.[19] Here it should be noted that the ordered magnetic moment of Fe given by the band-structure calculation, $3.88\mu_B$,[9] also agrees with the experimental value, suggesting that band theory gives correct ground-state properties of $CuFeS_2$.

D. Cu 3d states

In the Cu $2p$ XPS spectra of divalent and trivalent Cu compounds (Fig. 5), the main and satellite peaks are as-

signed to the $2p3d^{10}\underline{L}$ and $2p3d^9$ final states for CuO (Ref. 20) and to $2p3d^{10}\underline{L}^2$ and $2p3d^9\underline{L}$ final states for $NaCuO_2$.[21] In the Cu $2p$ XPS of monovalent or Cu^+ compounds, only the main peak is clearly observed because the Cu $3d$ shell is completely filled in the ground state and no ligand-to-$3d$ charge transfer is possible. In comparison with the spectrum of Cu_2O, we stated above that the Cu valence in both $CuFeS_2$ and $CuAl_{0.9}Fe_{0.1}S_2$ is Cu^+. From a careful inspection of the Cu $2p$ spectra, however, one notices in $CuFeS_2$ very weak humps around $E_B=945-948$ and 962–966 eV. Their energy difference from the main peak is 13–16 and 10–14 eV, respectively, which is much smaller than the peak energy of ~20 eV in the EELS spectrum (Figs. 12 and 13), thus excluding the possibility that the humps are originating from the bulk plasmon. Then we are led to consider the possibility that the Cu ion in $CuFeS_2$ has a small amount of divalent component in the ground state and that the humps are the satellites arising from the divalent component. In fact, such a weak divalent component has been found in the Cu^+ compound Cu_2O (see Fig. 5) and ascribed to the hybridization between the occupied Cu $3d$ states and the empty conduction band, which effectively leads to the mixing of the d^9 configuration into the d^{10} ground-state configuration.[14] The fact that the divalent component appears only in $CuFeS_2$ and not in $CuAl_{0.9}Fe_{0.1}S_2$ strongly suggests that the empty Fe $3d$ states are hybridized with the occupied Cu $3d$ states. Since the direct overlap between the Fe $3d$ and Cu $3d$ orbitals is unlikely because of the large atomic distance, we believe that the Fe $3d$–Cu $3d$ hybridization is mediated by the intervening S $3p$ valence-band states.

Now we consider the Cu $L_3M_{4,5}M_{4,5}$ Auger spectra. The two $3d$ holes produced by the Auger decay of the nominally d^{10} configuration form d^8 multiple states with components ^1S, ^3P, ^1D, ^3F, and ^1G.[22] The most intense peak in the spectra of Fig. 8 is due to the ^1G component. The effective Coulomb energy $U_{\rm eff}(^1G)$ between the two Cu $3d$ holes in the ^1G state can be estimated using the relation

$$U_{\rm eff}(^1G)=E_B(2p_{3/2})-E_{\rm kin}(^1G)-2E_B(3d)\ , \qquad (4)$$

where $E_{\rm kin}(^1G)$ is the kinetic energy of the ^1G Auger-electron component measured from the Fermi level. $E_B(2p_{3/2})$ and $E_B(3d)$ are the binding energies of the Cu $2p_{3/2}$ core level and the Cu $3d$ level, respectively,[20,23] deduced from the experimental data. $E_B(3d)$ is estimated to be 2.5 and 2.7 eV for $CuFeS_2$ and $CuAl_{0.9}Fe_{0.1}S_2$, respectively, from the valence-band XPS (Fig. 3).[24] The estimated values of $U_{\rm eff}(^1G)$ are 9.1 eV for $CuFeS_2$ and 10.1 eV for $CuAl_{0.9}Fe_{0.1}S_2$. The $U_{\rm eff}(^1G)$'s of Cu metal, CuCl, and $CuCl_2$ have been estimated in the same way[20,23] and are listed in Table I together with the width W of the Cu $3d$ band. The $U_{\rm eff}(^1G)$ and W are also plotted in Fig. 14, where they are found to lie on a straight line. If we plot the $U_{\rm eff}(^1G)$ of $CuFeS_2$ and $CuAl_{0.9}Fe_{0.1}S_2$ on this line, we obtain the Cu valence-band width of 2.5 and 2.0 eV, consistent with the valence-band photoemission spectra.[10] This result would again reflect the partial delocalization of the Cu $3d$ states in going from $CuAlS_2$ to $CuFeS_2$ as a result of the hybridization with the Fe $3d$ states.

TABLE I. Effective Coulomb energies $U_{\rm eff}(^1G)$ and the band widths W of the Cu $3d$ states. The results for $CuCl_2$, Cu metal, and CuCl are quoted from Ref. 22; the $U_{\rm eff}(^1G)$'s in the last two lines show the present results and the W's are obtained from the extrapolation of the W's of the first three substances.

	$U_{\rm eff}$ (eV)	W (eV)
$CuCl_2$	7	3.5
Cu metal	8	3.0
CuCl	10	2.0
$CuFeS_2$	9.1	2.5
$CuAl_{0.9}Fe_{0.1}S_2$	10.1	2.0

In the Cu $3p$ core excitation region, the Cu $3d$ valence bands of both compounds show only very weak resonance as seen in the lower panel of Fig. 11. On the other hand, clear resonance features are observed for the satellite around $E_B=15-16$ eV as shown in the upper panel of Fig. 11. Similar satellites have been observed in Cu^+ compounds, namely, Cu monohalides[25] and Cu_2O.[26] Instead of the direct recombination in the Cu^{2+} compounds following the Cu $3p\rightarrow 3d$ excitation, the $M_{2,3}M_{4,5}M_{4,5}$ super Coster-Kronig-type Auger decay occurs following the Cu $3p\rightarrow 4sp$ core excitation in the Cu^+ compounds, leading to the final-state configuration $(3d)^8(4sp)^1$. The binding energy $E_B(d^8{:}^1G)$ for this final state is given by[26,27]

$$E_B(d^8{:}^1G)=E_B(3d)+U_{\rm eff}(^1G)+\Delta_{d\text{-}sp}\ , \qquad (5)$$

where $E_B(3d)$ is the binding energy of the Cu $3d$ states[24] and $\Delta_{d\text{-}sp}$ is the promotion energy from the Cu $3d$ states to the bottom of the Cu $4sp$ conduction band. $U_{\rm eff}(^1G)$ between the two Cu $3d$ holes has been obtained from the Auger-electron spectra. Then $\Delta_{d\text{-}sp}$ is estimated to be 3.2 eV for $CuFeS_2$ and 3.1 eV for $CuAl_{0.9}Fe_{0.1}S_2$, which are comparable to the value (3 eV) for Cu_2O obtained using Eq. (5).[26] The bottom of the conduction band relative to

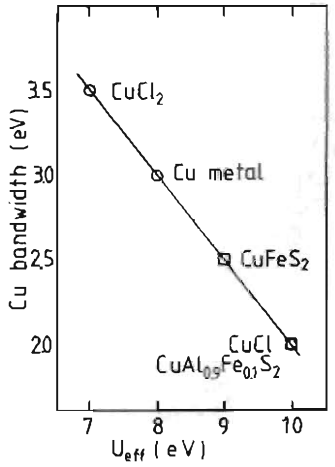

FIG. 14. Plot of the effective d-d Coulomb energies $U_{\rm eff}(^1G)$ and the bandwidths W of the Cu $3d$ states for various Cu compounds.

the top of the valence band is given by $\Delta_{d\text{-}sp} - E_B(3d)$ and is equal to 0.7 eV (=3.2–2.5 eV) for $CuFeS_2$ and 0.4 eV (=3.1–2.7 eV) for $CuAl_{0.9}Fe_{0.1}S_2$. The latter value is, however, somewhat too small compared to the optical band gap (3.3 eV) of $CuAlS_2$.[4,8] In order to treat this problem more accurately, consideration of hybridization between the S $3p$ and Cu $4sp$ states and a more accurate estimate of $U_{\text{eff}}(^1G)$ will be required.

V. CONCLUDING REMARKS

The electronic structures of $CuFeS_2$ and $CuAl_{0.9}Fe_{0.1}S_2$ have been studied by a combination of various electron and optical spectroscopic methods. The Fe $3d$ contribution in the valence-band region of $CuFeS_2$ is revealed by the difference spectrum between the XPS spectra of $CuFeS_2$ and $CuAl_{0.9}Fe_{0.1}S_2$. The Fe $3d$-derived spectrum including the satellite region is well reproduced by the CI calculation on the $(FeS_4)^{5-}$ cluster. The charge-transfer energy from the Fe $3d^5$ to $3d^6\underline{L}$ configurations has been estimated to be as small as $\Delta \sim 0$ eV or $\Delta_{\text{eff}} \sim 2$ eV, demonstrating the strong hybridization between the Fe $3d$ and S $3p$ states. The strong hybridization is consistent with the result of the Fe $3p$ core resonance photoemission spectroscopy and explains the reduced magnetic moment on the Fe atom and the high Neel temperature of $CuFeS_2$. The small tails observed on the larger E_B side of the Cu $2p$ and S $2p$ core spectra of $CuFeS_2$ are ascribed to the S $3p \rightarrow$Fe $3d$ interband excitation. Such a charge-transfer excitation is directly resolved in the optical reflectance and EELS spectra. The excitation energy is also consistent with the charge-transfer energy $\Delta_{\text{eff}} \sim 2$ eV between the lowest multiplet states of the d^5 and $d^6\underline{L}$ configurations.

The effective Coulomb energy $U_{\text{eff}}(^1G)$ between the two Cu $3d$ holes are estimated from the combination of the Cu $2p_{3/2}$ XPS, the Cu $L_3M_{4,5}M_{4,5}$ Auger-electron, and the Cu $3d$ valence-band XPS spectra. It is found that $U_{\text{eff}}(^1G)$ is larger for $CuAl_{0.9}Fe_{0.1}S_2$ than for $CuFeS_2$, reflecting the broader Cu $3d$ bandwidth in $CuFeS_2$. The observed hump on the larger binding energy side of the Cu $2p_{3/2}$ core level of $CuFeS_2$ is interpreted as a divalent satellite, indicating that a small amount of d^9 configuration is mixed into the d^{10} ground state in spite of the nominal valence Cu^+. This implies that the occupied Cu $3d$ states are appreciably hybridized with the empty Fe $3d$ states through their strong hybridization with the intervening S $3sp$ states.

We have successfully explained the principal features of both the spectroscopic and magnetic properties of $CuFeS_2$ and Fe-doped $CuAlS_2$ using the CI cluster-model calculation, while band theory explains the magnetic ground state of $CuFeS_2$. This indicates that both the Fe $3d$-$3d$ Coulomb interaction and the Fe $3d$–S $3p$ hybridization are essential to understand the present systems. Explicit calculations of the optical and magnetic properties, including the $d \rightarrow d$ absorption spectra, using the cluster model or the Anderson impurity model[16] will shed more light on their electronic structures. On the other hand, the Cu $3d$–Fe $3d$ hybridization as revealed by the present study may require more appropriate treatment of the extended electronic states beyond the cluster model. In the next step, band-structure effects which compete with the strong Coulomb correlation will have to be taken into account for further understanding of the physical properties including the transport phenomena. Concerning the question of whether $CuFeS_2$ is indeed a zero-gap semiconductor or not,[7] further experiments such as high-resolution photoemission studies in the vicinity of the Fermi level and combined photoemission-inverse-photoemission studies on well-characterized samples will be required.

ACKNOWLEDGMENTS

One of the authors (M.F.) would like to thank Professor T. Ishii and Professor S. Shin of the Synchrotron Radiation Laboratory of the Institute for Solid State Physics for valuable discussions. The authors are much obliged to the staff of Synchrotron Radiation Laboratory for technical support.

[1] J. L. Shay and J. H. Wernick, *Ternary Chalcopyrite Semiconductors, Growth, Electronic Properties and Applications* (Pergamon, New York, 1975).
[2] S. Kono and M. Okusawa, J. Phys. Soc. Jpn. **37**, 1301 (1974).
[3] T. Oguchi, T. Hamajima, T. Kambara, and K. Gondaira, Jpn. J. Appl. Phys. Suppl. **19-3**, 107 (1979).
[4] T. Teranishi, K. Sato, and K. Kondo, J. Phys. Soc. Jpn. **36**, 1618 (1974).
[5] T. Teranishi, J. Phys. Soc. Jpn. **16**, 1881 (1961).
[6] G. Donnay, L. M. Corliss, J. D. H. Donnay, N. Elliott, and J. M. Hastings, Phys. Rev. **112**, 1917 (1958).
[7] L. V. Kradinova, A. M. Polubotko, V. V. Popov, V. D. Prochukhan, Yu. V. Rud, and V. E. Skoriukin, Semicond. Sci. Technol. **8**, 1616 (1993).
[8] T. Oguchi, K. Sato, and T. Teranishi, J. Phys. Soc. Jpn. **48**, 123 (1980).
[9] T. Hamajima, T. Kambara, K. Gondaira, and T. Oguchi, Phys. Rev. B **24**, 3349 (1981).
[10] M. Fujisawa, M. Taniguchi, S. Shin, H. Daimon, H. Sakamoto, K. Sato, and S. Suga, in *Proceedings of the 18th International Conference on the Physics Semiconductors, Stockholm, 1987*, edited by O. Engstrom (World Scientific, Singapore, 1987), p. 1137.
[11] J. I. Yeh and I. Lindau, At. Data Nucl. Data Tables **32**, 1 (1985).
[12] N. Nucker, J. Fink, B. Renker, D. Ewert. C. Politis, J. W. P. Weijs, and J. C. Fuggle, Z. Phys. B **67**, 6 (1987).
[13] P. Steiner, V. Kinsinger, I. Sander, B. Siegwart, S. Hufner, C. Politis, R. Hoppe, and H. P. Muller, Z. Phys. B **67**, 497 (1987).
[14] K. Karlsson, O. Gunnarsson, and O. Jepsen, J. Phys. Condens. Matter **4**, 2801 (1992).
[15] A. Fujimori and F. Minami, Phys. Rev. B **30**, 957 (1984).
[16] T. Mizokawa and A. Fujimori, Phys. Rev. B **48**, 14 150 (1993).
[17] A. E. Bocquet, T. Mizokawa, T. Saitoh, H. Namatame, and A. Fujimori, Phys. Rev. B **46**, 3771 (1992); Solid State Commun.

83, 11 (1992).

[18]T. Hamajima *et al.* (Ref. 9) and private communication. The published band data in Ref. 9 were down to the binding energy of 7 eV as shown in Fig. 3. The calcualtion was performed down to about 15 eV, but no energy band is seen between $E_B=7$ and 15 eV except for the band assigned to the S 3*s* states at $E_B=14-15$ eV.

[19]J. Zaanen and G. A. Sawatzky, Can. J. Phys. **65**, 1262 (1987).

[20]G. van der Laan, G. A. Sawatzky, C. Haas, and H. W. Myron, Phys. Rev. B **20**, 4287 (1979).

[21]T. Mizokawa, H. Namatame, A. Fujimori, K. Akeyama, H. Kondoh, H. Kuroda, and N. Kosugi, Phys. Rev. Lett. **67**, 1638 (1991).

[22]E. Antonides, E. C. Janse, and G. A. Sawatzky, Phys. Rev. B **15**, 1669 (1977).

[23]G. van der Laan, C. Westra, C. Haas, and G. A. Sawatzky, Phys. Rev. B **23**, 4369 (1981).

[24]For $CuFeS_2$, we have adopted $E_B(3d)=2.5$ eV obtained from XPS [Fig. 3(b)] instead of $E_B(3d)=3.0$ eV from UPS (Figs. 1 and 9) because the Cu 3*d* cross section (2×10^{-2} Mb) is larger than the Fe 3*d* cross section (5×10^{-3} Mb) in XPS, while they are almost the same (~10 Mb) in UPS.

[25]T. Ishii, M. Taniguchi, A. Kakizaki, K. Naito, H. Sugawara, and I. Nagakura, Phys. Rev. B **33**, 5664 (1986), and references therein.

[26]J. Ghijsen, L. H. Tjeng, H. Eskes, and G. A. Sawatzky, Phys. Rev. B **42**, 2268 (1990).

[27]L. H. Tjeng, M. B. Meinders, J. van Elp, J. Ghijsen, and G. A. Sawatzky, Phys. Rev. B **41**, 3190 (1990).